

RSC Advances



This is an *Accepted Manuscript*, which has been through the Royal Society of Chemistry peer review process and has been accepted for publication.

Accepted Manuscripts are published online shortly after acceptance, before technical editing, formatting and proof reading. Using this free service, authors can make their results available to the community, in citable form, before we publish the edited article. This *Accepted Manuscript* will be replaced by the edited, formatted and paginated article as soon as this is available.

You can find more information about *Accepted Manuscripts* in the [Information for Authors](#).

Please note that technical editing may introduce minor changes to the text and/or graphics, which may alter content. The journal's standard [Terms & Conditions](#) and the [Ethical guidelines](#) still apply. In no event shall the Royal Society of Chemistry be held responsible for any errors or omissions in this *Accepted Manuscript* or any consequences arising from the use of any information it contains.

Copper(II) quinolinonato-7-carboxamido complexes as potent antitumor agents with broad spectrum and selective effects[†]

Radka Křikavová, Ján Vančo, Zdeněk Trávníček*, Roman Buchtík, Zdeněk Dvořák

Regional Centre of Advanced Technologies and Materials, Division of Biological Active Complexes and Molecular Magnets, Faculty of Science, Palacký University, 17. listopadu 12, CZ-771 46 Olomouc, Czech Republic. E-mail: zdenek.travnicek@upol.cz.

RSC Advances Accepted Manuscript

[†] Electronic supplementary information (ESI) available: Fig. S1. ¹H and ¹³C NMR spectra of Hqui⁴. Fig. S2. Mid-FTIR spectra of Hqui⁴ (up) and complex **4** (down). Fig. S3. The electrophoreogram depicting the interactions of complexes **1** (lanes 1–3), **2** (lanes 4–6), **3** (lanes 7–9), and **5** (lanes 10–12) applied at 200 μM concentration with pUC19 plasmid DNA. Blank sample contained only the native form of pUC19 plasmid DNA (lane 13). Fig. S4. Dose-viability curves for complexes **1-3** and **5**. See DOI: ...

Abstract

A series of five copper(II) mixed-ligand complexes with the composition $[\text{Cu}(\text{qui}^x)(\text{phen})]\text{NO}_3 \cdot y\text{H}_2\text{O}$ (**1–5**), where Hqui^x stands for 2-(4-amino-3,5-dichlorophenyl)-3-hydroxy-4(1*H*)-quinolinone-7-carboxamides with *N*-substitution: $\text{Hqui}^1 = N$ -propyl (**1**), $\text{Hqui}^2 = N$ -isobutyl (**2**), $\text{Hqui}^3 = N$ -cyclohexyl (**3**), $\text{Hqui}^4 = N$ -benzyl (**4**), $\text{Hqui}^5 = N$ -*p*-xylyl (**5**); *phen* = 1,10-phenanthroline and $y = 0–1$, was synthesized, characterized and screened for *in vitro* antitumor activity on a panel of six human cancer cell lines, including osteosarcoma (HOS), breast adenocarcinoma (MCF7), malignant melanoma (G361), cervix carcinoma (HeLa), ovarian carcinoma (A2780) and *cisplatin*-resistant ovarian carcinoma (A2780R). All the complexes, except for limitedly soluble **4**, showed very potent cytotoxicity ($\text{IC}_{50} \approx 1–7 \mu\text{M}$), with the best IC_{50} value for complex **5** against A2780, with $\text{IC}_{50} = 0.6(1) \mu\text{M}$. Moreover, complex **5** was found to be non-toxic up to 50 μM against non-malignant lung fibroblast cells (MRC-5), therefore showing a promising selectivity index [$\text{IC}_{50}(\text{MRC-5})/\text{IC}_{50}(\text{A2780})$] higher than 80. The complexes were also shown to bind to calf-thymus DNA, interact with the physiological levels of L-cysteine and act as chemical nucleases. It was additionally suggested that the species responsible for the biological activities of the prepared complexes were represented by the cations $[\text{Cu}(\text{qui})(\text{phen})]^+$, or similar cationic species containing the $\{\text{Cu}(\text{phen})\}$ residue. The results clearly demonstrated that targeted structural optimization of the quinolinonato ligand in this class of complexes leads to the compounds with high-level and broad-spectrum anticancer activity, and at the same time with significantly increased selectivity.

Keywords: Copper(II) mixed-ligand complexes; Quinolinone-7-carboxamides; *In vitro* cytotoxicity; DNA interactions; Antitumor activity; Nuclease activity.

1. Introduction

Metal-based cancer therapy has hitherto exploited the antitumour properties of exclusively platinum(II) complexes. Concretely, *cisplatin* and its derivatives (*oxaliplatin*, *carboplatin* etc.) are currently well-established anticancer drugs used worldwide, whose therapeutic effect is based on the inhibition of cancer cell proliferation through binding to nuclear DNA.¹⁻³ However, these platinum(II) complexes possess several limitations complicating chemotherapy, such as negative side-effects (e.g. neurotoxicity, nephrotoxicity and emetogenesis) and intrinsic and/or acquired resistance phenomena.^{4,5} Nevertheless, it is unambiguously the high therapeutic efficiency of these platinum(II)-based therapeutics, which has inspired many scientists to focus on the development of next generations of transition metal complexes with an improved anticancer profile and simultaneously with reduced negative side-effects.⁶ One of the investigated approaches to decreasing the toxicity with respect to the platinum(II) complexes involves using essential transition metals as central atoms. Copper has been identified as a promising candidate, as it is an essential trace element found in all living organisms. It is involved in multiple functions of crucial enzymes⁷ and works as a fundamental component of the redox system (transition between the Cu^I and Cu^{II} oxidation states).⁸ Furthermore, the benefit of copper being an endogenous essential metal additionally lies in the already established metabolism pathways for copper-containing compounds, which could also play a role in modulating the general toxicity of prospective copper-based therapeutics.

The advantages of using copper as the central atom for the preparation of potential metallotherapeutics have already been exemplified on a number of copper complexes, particularly involving a planar polyheterocyclic ligand, which have shown notable cytotoxicity with the mechanism of action related to varied modes of DNA interactions and redox metabolism alterations.⁹⁻¹² The first reported Cu^{II} complex of this group able to inhibit tumour growth *in vivo* (studied on the model of Landschutz ascites tumour in mice) was shown to have the composition [Cu(*tmphen*)₂]Cl₂, where *tmphen* stands for 3,4,7,8-tetramethyl-1,10-phenanthroline.¹³ Since then,

many Cu^{II} complexes containing 1,10-phenanthroline (*phen*) and other bidentate *N*-donor heterocyclic ligands (N-N) and bidentate *O*-donor ligands (O-O) of the type [Cu(N-N)(O-O)]^{n=0/1+} have been synthesized and studied for their anticancer properties. Among these compounds, Cu^{II} mixed-ligand bis-chelated antineoplastic agents, containing *phen*, 2,2'-bipyridine (*bpy*) or their substituted derivatives and essential amino acids or acetylacetonone,¹⁴⁻¹⁸ called Casiopeínas[®], stand out. Their remarkable antitumour activity *in vitro*, *in vivo* and promising results from preclinical studies have classified the complexes as auspicious candidates for clinical trials.¹⁹

In our recent works, we have focused on the Casiopeínas[®]-like mixed-ligand Cu^{II} complexes, containing a bidentate *N*-donor heterocyclic ligand (*phen*, *bpy*, or their derivatives, N-N), the 2-phenyl-3-hydroxy-4(1*H*)-quinolinonato ligand (*qui*) and nitrate or tetrafluoroborate counter anions (Y), of the general composition [Cu(*qui*)(N-N)]Y·*y*H₂O.²⁰⁻²² The complexes were identified as promising cytotoxic agents on a broad spectrum of human cancer cell lines, with IC₅₀ reaching micromolar to sub-micromolar values, e.g. the IC₅₀ value against ovarian cancer cells A2780 equalled 0.36±0.05 μM for [Cu(*qui*)(*mphen*)]BF₄·H₂O (*mphen* = 5-methyl-1,10-phenanthroline). Moreover, markedly lower cellular toxicity of the complexes to healthy cells was observed, with the ratio between the effective concentration against the cancer cells and toxic concentration to primary human hepatocytes of up to 1:40. Generally, the best selectivity index was observed for the complexes involving non-substituted *phen* as the *N*-donor ligand.

Quite recently, an extensive structure-cytotoxic activity relationship study has been performed for 2-phenylsubstituted-3-hydroxyquinolin-4(1*H*)-one-carboxamides, which showed that the carboxamide substitution plays a positive role in tuning of cytotoxicity (the best derivatives showed submicromolar IC₅₀ values against CEM leukaemia cell line) and resulted in a very favourable therapeutic index (up to 40 for the derivatives used in this study).²³ These encouraging results inspired us to extend our previous studies and elucidate whether and how the 2-(3,5-dichloro-4-amino)phenyl- and 7-alkylcarboxamido-substitution on the quinolinone skeleton may influence the biological activity of the mixed-ligand complexes of the [Cu(*qui*^x)(*phen*)]NO₃·*y*H₂O (1–5) type. Herein,

we report on the synthesis, thorough characterization and results of biological activity evaluation, i.e. cytotoxicity screening against a panel of seven human cancer and non-malignant cell lines, investigations of their interactions with DNA and sulphur-containing biomolecules, of a series of copper(II) complexes of the general composition $[\text{Cu}(\text{qui}^x)(\text{phen})]\text{NO}_3 \cdot y\text{H}_2\text{O}$ (**1–5**, where $x = 1-5$, $y = 0$ or 1).

2. Experimental

2.1. Materials and methods

Chemicals and solvents were purchased from Sigma-Aldrich Co. and Acros Organics Co., and were used as received. The 2-phenyl-3-hydroxy-4(1*H*)-quinolinone-7-carboxamides (Hqui^{1-5}) with *N*-substitution: $\text{Hqui}^1 = N$ -propyl, $\text{Hqui}^2 = N$ -isobutyl, $\text{Hqui}^3 = N$ -cyclohexyl, $\text{Hqui}^4 = N$ -benzyl, $\text{Hqui}^5 = N$ -*p*-xylyl, used as the starting materials for the preparation of complexes **1–5** were synthesized following the formerly reported procedure²⁴ and their purity was verified by elemental analysis, FTIR and NMR spectroscopy (Figs. S1 and S2, ESI).

Elemental analysis (C, H, N) was carried out on a Flash EA-2000 Elemental Analyser (ThermoFinnigan). FTIR spectra were recorded on a Nexus 670 FTIR (ThermoNicolet) using the ATR technique in the range of 200–4000 cm^{-1} . Electronic absorption spectra of 10^{-3} and 10^{-5} M *N,N*-dimethylformamide (DMF) solutions and diffuse-reflectance UV-Vis spectra were recorded with a Lambda 40 spectrometer (Perkin Elmer instruments) in the range of 300–900 nm. Mass spectra (MS) were recorded on an LCQ Fleet (ThermoFisher Scientific) spectrometer using the positive electrospray ionisation (ESI+) and full scan mode for the 10^{-5} M methanol solutions of **1–5**. NMR spectra of Hqui^{1-5} were measured in $\text{DMF-}d_7$ on a Varian 400 MHz NMR spectrometer at 298 K. Tetramethylsilane (TMS) was used as the internal reference standard for ^1H and ^{13}C NMR experiments. Simultaneous thermogravimetric (TG) and differential thermal (DTA) analyses were performed on a thermal analyser Exstar TG/DTA 6200 (Seiko Instruments Inc.). TG/DTA studies were carried out in platinum pans from ambient temperature to 800 °C with a 2.5 °C min^{-1} temperature

gradient in dynamic air atmosphere (100 mL min⁻¹). Conductivity experiments were performed on a Cond 340i/SET (WTW) in DMF (10⁻³ M, at 25 °C). The quantum chemical calculations were performed at the DFT-level using the hybrid B3LYP functional with the LACVP+** basis set using the Spartan'10 (version 1.1.0v4) software.²⁵⁻²⁷

2.2. Synthesis of [Cu(*qui*¹)(*phen*)]NO₃ (1), [Cu(*qui*²)(*phen*)]NO₃ (2), [Cu(*qui*³)(*phen*)]NO₃ (3), [Cu(*qui*⁴)(*phen*)]NO₃·H₂O (4) and [Cu(*qui*⁵)(*phen*)]NO₃ (5).

1,10-phenanthroline (*phen*) monohydrate (198 mg, 1 mmol) was dissolved in ethanol (10 mL) and then, the corresponding quinolinone (*Hqui*¹⁻⁵) (1 mmol) dispersed in ethanol (30 mL) was added while stirring. A solution of Cu(NO₃)₂·3H₂O (242 mg, 1 mmol) in distilled water (5 mL) was slowly added to the resulting mixture while stirring. The reaction mixture was stirred at room temperature for a few hours until a solid product formed. The obtained solid was filtered off, washed with a small amount of cold water and ethanol, and dried at 40 °C under an infrared lamp.

[Cu(*qui*¹)(*phen*)]NO₃ (1) (565 mg, 79.5%). Found: C, 52.3; H, 3.8.; N, 11.4%. Calc. for C₃₁H₂₄N₆O₆Cl₂Cu (M_r = 711.0): C, 52.4; H, 3.4; N, 11.8%. TG/DTA: the decomposition began at 202 °C with subsequent exothermic effects with the maxima centred at 266, 282, 329 and 506 °C, and finished at 537 °C. Λ_m (S cm² mol⁻¹): 70 (electrolyte 1:1). λ_{max} (solid state)/nm 445, 739. λ_{max} (10⁻⁵ M DMF solution)/nm) 425 (ε/M⁻¹ cm⁻¹ 9288). FTIR (ν, cm⁻¹): 3307, 3200, 3070, 2961, 2934, 2874, 1664, 1623, 1572, 1541, 1492, 1452, 1429, 1376, 1314, 1254, 1184, 1148, 1040, 943, 895, 878, 847, 742, 720, 697, 653, 601, 584, 561, 513, 432, 337, 311, 244. ESI+ MS: *m/z* 647 ([M-(NO₃)]⁺, 100%), 243 ([Cu(*phen*)]⁺, 10%), 1296 ([{M-(NO₃)₂}]⁺, 2%).

[Cu(*qui*²)(*phen*)]NO₃ (2) (615 mg, 84.8%). Found: 52.7; H, 3.6; N, 11.6%. Calc. for C₃₂H₂₆N₆O₆Cl₂Cu (M_r = 725.0): C, 53.0; H, 3.6; N, 11.6%. TG/DTA data: the decomposition began at 186 °C with subsequent exothermic effects with the maxima at 266, 282, 338 and 522 °C, and finished at 587 °C. Λ_m (S cm² mol⁻¹): 70 (electrolyte 1:1). λ_{max} (solid state)/nm 445, 751. λ_{max} (10⁻⁵ M DMF solution)/nm 437 (ε/M⁻¹ cm⁻¹ 8470). FTIR (ν, cm⁻¹): 3311, 3238, 3200, 3068, 2959, 2930, 2872, 1624, 1575, 1543, 1490,

1453, 1431, 1372, 1312, 1257, 1184, 1146, 1087, 1042, 942, 894, 878, 847, 744, 720, 693, 655, 600, 582, 560, 501, 434, 335, 311. ESI+ MS: m/z 661 ($[M-(NO_3)]^+$, 100%), 1322 ($\{[M-(NO_3)]_2\}^+$, 30%), 243 ($[Cu(phen)]^+$, 18%).

[Cu(*qui*³)(*phen*)]NO₃ (3) (598 mg, 79.6%). Found: C, 54.1; H, 3.7; N, 11.0%. Calc. for C₃₄H₂₈N₆O₆Cl₂Cu (M_r = 751.1): C, 54.4; H, 3.8; N, 11.2%. TG/DTA: the decomposition began at 188 °C with subsequent exothermic effects with the maxima centred at 275, 283, 327 and 482 °C, and finished at 545 °C. Λ_m (S cm² mol⁻¹): 65 (electrolyte 1:1). λ_{max} (solid state)/nm 425, 789. λ_{max} (10⁻⁵ M DMF solution)/nm) 424 ($\epsilon/M^{-1} \text{ cm}^{-1}$ 12660). FTIR (ν , cm⁻¹): 3319, 3109, 3068, 2930, 2855, 1620, 1573, 1544, 1520, 1494, 1453, 1431, 1376, 1314, 1255, 1182, 1150, 1111, 1082, 1040, 943, 892, 876, 848, 830, 789, 742, 722, 698, 653, 619, 588, 563, 495, 471, 436, 332, 310, 259. ESI+MS: m/z 687 ($[M-(NO_3)]^+$, 100%), 1376 ($\{[M-(NO_3)]_2\}^+$, 15%), 243 ($[Cu(phen)]^+$, 9%).

[Cu(*qui*⁴)(*phen*)]NO₃·H₂O (4) (535 mg, 70.5%). Found: C, 53.9; H, 3.4; N, 10.5%. Calc. for C₃₅H₂₄N₆O₆Cl₂Cu·H₂O (M_r = 777.1): C, 54.1; H, 3.4; N, 10.8%. TG/DTA: a weight loss of 2.4% is accompanied by an endothermic effect with the minimum at 90 °C (2.3% calcd. for H₂O); the decomposition of the non-solvated complex began at 196 °C with subsequent exothermic effects with the maxima centred at 259, 288, 332 and 472 °C, and finished at 577 °C. Λ_m (S cm² mol⁻¹): 70 (electrolyte 1:1). λ_{max} (solid state)/nm 451, 778. λ_{max} (10⁻⁵ M DMF solution)/nm) 427 ($\epsilon/M^{-1} \text{ cm}^{-1}$ 10129). FTIR (ν , cm⁻¹): 3456, 3319, 3198, 3084, 3063, 3034, 3007, 2967, 2930, 1619, 1572, 1542, 1378, 1308, 1253, 1226, 1180, 1145, 1109, 1082, 1039, 946, 889, 876, 845, 790, 740, 720, 698, 653, 603, 565, 557, 514, 501, 460, 435, 413, 303, 247. ESI+ MS: m/z 695 ($[M-(NO_3)]^+$, 100%), 1390 ($\{[M-(NO_3)]_2\}^+$, 20%), 243 ($[Cu(phen)]^+$, 10%).

[Cu(*qui*⁵)(*phen*)]NO₃ (5) (524 mg, 67.8%). Found: C, 55.6; H, 3.4; N, 10.7%. Calc. for C₃₆H₂₆N₆O₆Cl₂Cu (M_r = 773.1): C, 55.9; H, 3.4; N, 10.9%. TG/DTA: the decomposition began at 173 °C with subsequent exothermic effects with the maxima centred at 264, 291, 335 and 504 °C, and finished at 584 °C. Λ_m (S cm² mol⁻¹): 65 (electrolyte 1:1). λ_{max} (solid state)/nm 448, 773. λ_{max} (10⁻⁵ M DMF solution)/nm) 424 ($\epsilon/M^{-1} \text{ cm}^{-1}$ 10941). FTIR (ν , cm⁻¹): 3331, 3066, 2946, 2924, 2863, 1621, 1575, 1545, 1492, 1455,

1429, 1381, 1312, 1279, 1252, 1227, 1181, 1147, 1111, 1040, 947, 894, 878, 848, 785, 759, 742, 722, 694, 655, 615, 584, 565, 492, 477, 436, 344, 318, 246. ESI+ MS: m/z 709 ($[M-(NO_3)]^+$, 100%), 1418 ($[{M-(NO_3)}_2]^+$, 23%), 243 ($[Cu(phen)]^+$, 11%).

2.3. Biological activity

2.3.1. *In vitro* cytotoxicity testing

The Cu^{II} complexes **1–5** together with *cisplatin*, the antineoplastic drug used as a reference standard, were evaluated for their *in vitro* cytotoxicity by the MTT (3-(4,5-dimethylthiazol-2-yl)-2,5-diphenyltetrazolium bromide) assay against six human cancer cell lines, namely osteosarcoma (HOS; ECACC No. 87070202), breast adenocarcinoma (MCF7; ECACC No. 86012803), cervix epitheloid carcinoma (HeLa; ECACC No. 93021013), malignant melanoma (G361; ECACC No. 88030401), ovarian carcinoma (A2780; ECACC No. 93112519), *cisplatin*-resistant ovarian carcinoma (A2780R; ECACC No. 93112517), and non-malignant human foetal lung fibroblast cells (MRC-5; ECACC No. 84101801). The cell lines were purchased from the European Collection of Cell Cultures (ECACC; Prague, Czech Republic). The cells were maintained in a humidified incubator (37 °C, 5% CO₂). The cells were treated with the tested compounds (**1–5** and *cisplatin*) at the 0.01, 0.1, 1.0, 5.0, 25.0 and 50 µM concentrations for 24 h, using multi-well culture plates of 96 wells. In parallel, the cells were treated with vehicle (DMF; 0.1% v/v) and Triton X-100 (1% v/v) to assess the minimal (*i.e.* positive control) and maximal (*i.e.* negative control) cell damage, respectively. The cells were incubated with MTT for 3–4 h, after removal of the medium and washing the cells with the phosphate buffer solution, formazan dye was dissolved in DMF containing 1% of ammonia. The MTT assay absorbance was measured spectrophotometrically at 540 nm (TECAN, Schoeller Instruments LLC). The data were expressed as the percentage of viability, when 100% and 0% represent the treatments with DMF, and Triton X-100, respectively.²¹ The cytotoxicity data from the cell lines were obtained from three independent experiments using the cells from different passages, while each experiment was performed in triplicate. The obtained IC₅₀±SD (µM) values together with their standard deviations

(SD) were calculated from the dose-viability curves by linear regression analysis of the area containing the steepest and almost linear descent of the curve. (see the dose-viability curves in ESI, Fig. S4). The significance of the differences between the results was assessed by the ANOVA analysis, with $p < 0.05$ considered to be significant.²⁸

2.3.2. Interaction with calf thymus DNA (CT-DNA) assessed by the fluorescence titration

Interaction with calf-thymus (CT)-DNA was assessed by the fluorescence ethidium bromide (EB) displacement assay. Fluorescence quenching experiments were performed in the Tris/HCl buffer [tris(hydroxymethyl) aminomethane], containing 5 mM Tris and 50 mM NaCl, adjusted to pH 7.2 by the addition of HCl and carried out by the addition of the complexes to a sample solution containing EB-DNA. The spectra were recorded at the excitation wavelength of 520 nm for an emission range of 550–750 nm. In the fluorescence quenching spectra, the reduction in emission intensity measures the binding propensity of the complex to CT-DNA. The Stern–Volmer quenching constant (K_{sv}) and the apparent binding constant (K_{app}) were calculated using the equations $F_0/F = 1 + K_{sv} r$ and $K_{EB} [EB] = K_{app}[\text{Complex}]$, where F_0 and F correspond to the fluorescence intensities of EB–DNA in the absence and presence of the complex, respectively, r is the ratio of the total concentration of the complex to that of DNA, and $K_{EB} = 1 \times 10^7 \text{ M}^{-1}$, $[EB] = 5 \text{ } \mu\text{M}$ and $[\text{Complex}]$ is the concentration of the complex at a 50% reduction of the emission intensity of EB.²⁹

2.3.3. pUC19 plasmid DNA cleavage

Supercoiled plasmid DNA, pUC19 (2686 bp, 1750 kDa), was obtained from Invitrogen, Netherlands, solubilised in storage buffer (10 mM Tris-HCl, 5 mM NaCl, 0.1 mM EDTA, pH= 7.4, 250 $\mu\text{g}/\text{mL}$). Supercoiled plasmid pUC19 (300 ng per reaction, corresponding to the concentration of 23 μM calculated to base pairs) was mixed with different concentrations (20 μM , 100 μM , and 200 μM) of the selected representative complex **5** (in different setups, either in the presence, or in the absence of the reducing agent L-ascorbic acid (at the 1.66 mM concentration)) in TBE buffer (containing 89

mM Tris, 89 mM boric acid, and 2 mM EDTA). The reaction mixtures were incubated at 37 °C for 1 h and then analysed by 0.8% agarose gel electrophoresis and detected with EB staining. The electrophoreogram was analysed by the software AlphaEaseFC, version 4.0.0.34 (Alpha Innotech, USA) and the relative percentages of circular (CCC), one strand nicked (OC), and linear (L) forms were evaluated. The quantitative parameter of total DNA cleavage was calculated as the percentage of the integrated density of cleaved forms (OC-form + 2 x L-form) from the sum of integrated densities of all identified forms of DNA (CCC-form + OC-form+ 2 x L-form). Each experiment was performed in triplicate and the presented results are mean values calculated from all the experiments.

2.3.4. Interactions with sulphur-containing biomolecules assessed by ESI-MS

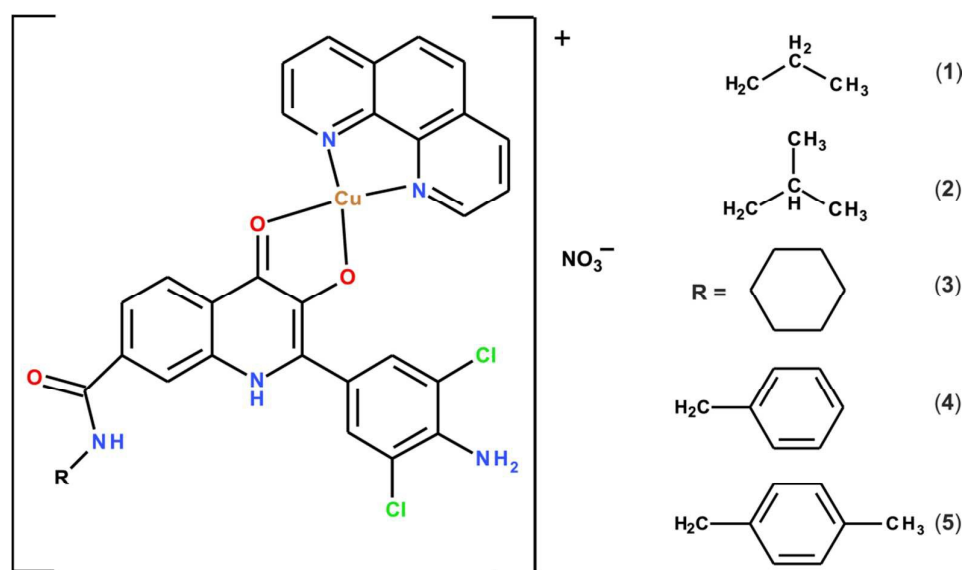
The interaction experiments between the representative complex **5** and the mixture of physiological levels of L-cysteine and L-glutathione (290 µM, and 6 µM, respectively)³⁰ were performed on a ThermoFinnigan LTQ Fleet Ion-Trap mass spectrometer, using the positive ionization mode. The flow-injection analysis method was used to introduce the reaction system (20 µL spikes) into the mass spectrometer, while the acetonitrile (gradient grade) was used as a mobile phase. The ESI- source was set up as follows: source voltage was 4.9 kV, the vaporizer temperature was 160°C, the capillary temperature was 275 °C, the sheath gas flow rate was 20 L/min, and auxiliary gas flow rate was 5 L/min. The system was calibrated according to the manufacturer specifications and no further tuning was needed. In addition, the solutions, containing the mixture of L-cysteine and L-glutathione and the solution of complex **5** in methanol/water (1:1, v/v), were used as reference samples. The interacting system was analysed immediately after preparation (0 h), and then 1, 12, and 24 h after the solutions of complex **5** and sulphur-containing biomolecules were mixed.

3. Results and Discussion

3.1. General properties

The yellow-green copper(II) complexes of the general composition $[\text{Cu}(\text{qui}^{1-5})(\text{phen})]\text{NO}_3 \cdot x\text{H}_2\text{O}$ (**1–5**; $x = 0–1$) were synthesized *via* the reaction of 1,10-phenanthroline (*phen*) monohydrate and the corresponding 2-(4-amino-3,5-dichlorophenyl)-3-hydroxy-4(1*H*)-quinolinone-7-carboxamide with *N*-substitution, i.e. $\text{Hqui}^1 = N$ -propyl (**1**), $\text{Hqui}^2 = N$ -isobutyl (**2**), $\text{Hqui}^3 = N$ -cyclohexyl (**3**), $\text{Hqui}^4 = N$ -benzyl (**4**), $\text{Hqui}^5 = N$ -*p*-xylyl (**5**), with $\text{Cu}(\text{NO}_3)_2 \cdot 3\text{H}_2\text{O}$ in an ethanol/water mixture (11 : 1, v/v) in the 1 : 1 : 1 molar ratio, with the yields of 68–85% (Scheme 1). According to the conductivity measurements, complexes **1–5** behaved as electrolytes of the 1 : 1 type in 10^{-3} M DMF solutions with the conductivity values of ca. $70 \text{ S cm}^2 \text{ mol}^{-1}$. Further, all the ESI+ mass spectra of the studied compounds contained the peaks of the corresponding complex $[\text{Cu}(\text{qui}^{1-5})(\text{phen})]^+$ cations with the relative intensity of 100%, thus providing evidence about the composition of **1–5**. Additionally, the peaks of the fragments of the dimeric species $\{[\text{Cu}(\text{qui}^{1-5})(\text{phen})]_2\}^+$ as well as a peak corresponding to $[\text{Cu}(\text{phen})]^+$ at 243.0 m/z (calc. 243.0) were detected in the spectra of all the complexes, thus suggesting the same fragmentation patterns for the studied compounds.

The presence of the water molecule of crystallization in the monohydrated complex **4** was confirmed by the simultaneous TG/DTA analysis. The calculated and experimental data regarding the crystal water elimination was found to be in good accordance (calcd./found 2.4/2.3%). All the other complexes were found thermally stable up to ca. 180-200 °C. The course of the thermal degradation of all the complexes above 200 °C was analogical, proceeding without the formation of any thermally stable intermediates, and characterized by four exothermic effects on the DTA curve. The final product of degradation (probably associated with the formation of CuO) formed at ca. 540-580 °C. The thermal decomposition data are listed in Section 2.3.



Scheme 1 A general structural formula of complexes **1–5**.

3.2. UV-Vis and FTIR spectral characterizations

The electronic spectra of the Cu^{II} complexes **1–5** were measured in the 300–900 nm region, both in the solid state and DMF solutions (10^{-3} and 10^{-5} M). The diffuse-reflectance spectra of the complexes exhibited one intensive well-defined absorption maximum centred at 425–451 nm, assignable to charge-transfer transitions (CT), and one very broad maximum in the range of 739–789 nm, which could be attributed to $d-d$ transitions of the ${}^2B_{1g} \rightarrow {}^2E_g$, ${}^2B_{1g} \rightarrow {}^2B_{2g}$, and ${}^2B_{1g} \rightarrow {}^2A_{1g}$ types characteristic of copper(II) complexes with a distorted square-planar arrangement.³¹ The UV-Vis spectra of **1–5** measured in the 10^{-5} DMF solutions were dominated by CT transitions observed in a similar region, at 425 nm (**1**), 437 nm (**2**), 424 nm (**3**), 427 nm (**4**) and 424 nm (**5**). The maxima corresponding to the $d-d$ transitions with low absorbance values could be detected as unintensive shoulder bands only in the DMF solutions with $c \geq 10^{-3}$ M. In comparison with the solid state spectra, these maxima were shifted to lower wavelengths ranging from 599 to 611 nm (molar absorption coefficients equalling 81–156 $\text{M}^{-1} \text{cm}^{-1}$) (Fig. 1). This shift is most likely connected with a change in the coordination geometry around the metal as a result of the coordination of solvent molecules to the copper(II) centre in the

solution, which was confirmed by means of EPR spectroscopy for structurally analogical complexes in our previous work.²⁰

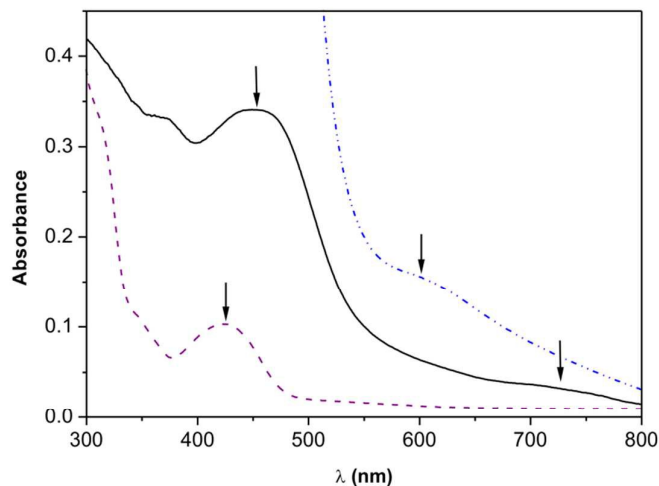


Fig. 1 UV-Vis spectra of complex **1** in the range of 300-800 nm: Diffuse reflectance spectrum (solid black line); 10^{-5} M DMF solution spectrum (violet dashed line); 10^{-3} M DMF solution spectrum (blue dash-dotted line). λ_{\max} (solid state, nm): 445, 739. λ_{\max} (10^{-5} M DMF solution, nm)/ ϵ ($M^{-1} \text{ cm}^{-1}$): 425/9288. λ_{\max} (10^{-3} M DMF solution, nm)/ ϵ ($M^{-1} \text{ cm}^{-1}$): 605/156. Maxima displayed as black arrows.

The FTIR spectra were recorded in the region of $150\text{--}4000 \text{ cm}^{-1}$. The interpretation of the spectra, made also in comparison with the spectra of *Hqui*¹⁻⁵ and *phen*, indirectly confirmed the coordination of both types of organic ligands to the copper(II) atom. In the region of $2800\text{--}3500 \text{ cm}^{-1}$, there were identified bands of the characteristic stretching vibrations of the types $\nu(\text{N-H})$ at $3307\text{--}3331 \text{ cm}^{-1}$, $\nu(\text{C-H})_{\text{ar}}$ at $3063\text{--}3109 \text{ cm}^{-1}$, $\nu(\text{C-H})_{\text{aliph}}$ at $2855\text{--}2959 \text{ cm}^{-1}$. The spectrum of monohydrated complex **4** additionally showed a broad band at 3456 cm^{-1} assignable to $\nu(\text{O-H})$ originating from the water molecule of crystallization. Further, there were two characteristic bands of a carbonyl group clearly observed in the spectra of **1–5**. A weak to medium intensity band in the region of $1642\text{--}1664 \text{ cm}^{-1}$ could be assigned to the stretching amide carbonyl vibration, while the strong bands at $1619\text{--}1624 \text{ cm}^{-1}$ are assignable to the *qui* carbonyl group in the position 4 of the heterocycle. The aromatic

$\nu(\text{C}=\text{C})_{\text{ring}}$ vibrations of the *phen* ring can be found between 1572–1575 cm^{-1} and in the region of 1429–1431 cm^{-1} . Very strong characteristic bands of the *qui* aromatic $\nu(\text{C}=\text{C})_{\text{ring}}$ vibrations appeared at 1490–1494 cm^{-1} . The band of the medium intensity in the region of 1372–1381 cm^{-1} should be assigned to *qui* $\nu(\text{CNH})$ vibration. The uncoordinated nitrate group $\nu_3(\text{NO}_3)$ bands were observed between 1308–1314 cm^{-1} . There were also detected two bands at 845–848 and 720–722 cm^{-1} which are characteristic of the *phen* ligand (Fig. S2, ESI). In the far-IR region, the medium bands at 303–318 cm^{-1} could be attributed to $\nu(\text{Cu-N})$, whereas the peaks at 560–565 and 492–513 cm^{-1} could be connected with the stretching vibrations of $\nu(\text{Cu-O})$.³²⁻³⁴

3.3. Quantum chemical calculations

The X-ray structures of two complexes $[\text{Cu}(\text{qui})(\text{phen})]\text{NO}_3 \cdot \text{H}_2\text{O}$ and $[\text{Cu}(\text{qui})(\text{ambpy})]\text{NO}_3$ (*ambpy* = bis(2-pyridyl)amine) with analogical compositions to **1–5** have been already reported.²⁰ Although several attempts (including slow evaporation of the reaction solution or mother liquor at varied temperatures, diffusion of diethyl ether to saturated ethanol/DMF solution) were made in order to obtain suitable crystals of **1–5** for a single crystal X-ray analysis, all employed methods were unsuccessful. In the effort to confirm the composition of **1–5** suggested by the results of various analytical methods described above and to predict the molecular structure of the prepared complexes, a model for DFT calculation was built on the basis of the structural similarity with $[\text{Cu}(\text{qui})(\text{phen})]\text{NO}_3 \cdot \text{H}_2\text{O}$ and $[\text{Cu}(\text{qui})(\text{ambpy})]\text{NO}_3$.²⁰ The geometry of the complex cation of **3** was optimized at the DFT level using the hybrid B3LYP functional with the LACVP+** basis set. The optimized geometry of $[\text{Cu}(\text{qui}^3)(\text{phen})]^+$ is shown in Fig. 2. The copper(II) atom is tetra-coordinate by one bidentate *O,O*-coordinated *qui*³ (*Hqui*³ = 2-(4-amino-3,5-dichlorophenyl)-*N*-cyclohexyl-3-hydroxy-4(1*H*)-quinolinone-7-carboxamide) and one bidentate *N,N*-coordinated *phen*. The Cu–N bond lengths (Cu–N1 = 2.043 Å; Cu–N2 = 2.043 Å) were found to be rather longer than Cu–O (Cu–O1 = 1.916 Å; Cu–O2 = 1.941 Å), which is in agreement with the bond length comparison in the vicinity of the metal centre in the structurally related complex $[\text{Cu}(\text{qui})(\text{phen})]\text{NO}_3 \cdot \text{H}_2\text{O}$ (further abbreviated as CuQ).²⁰

However, the calculated bond lengths in the vicinity of the central atom were found to be slightly longer than those found in the X-ray structure of CuQ (Cu–N1 = 1.988(2) Å; Cu–N2 = 1.978(2) Å; Cu–O1 = 1.892(2) Å; Cu–O2 = 1.916(2) Å). The geometry around the copper(II) atom in **4** could be described as a distorted square-planar; the angles O1–Cu–N1 and O2–Cu–N2 were equal to 177.28°, and 175.34°, respectively.

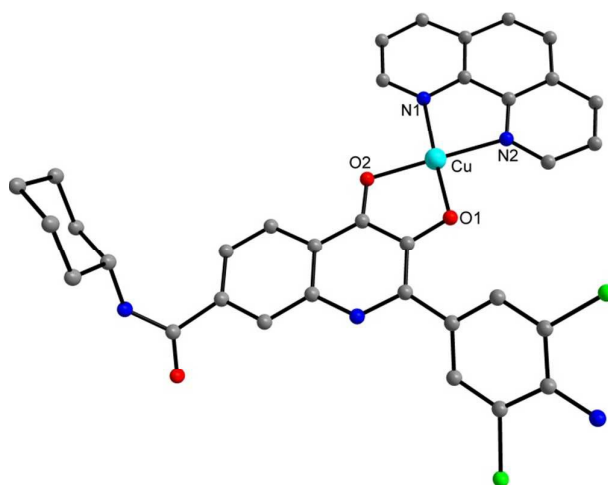


Fig. 2 The geometry of the complex $[\text{Cu}(\text{qui}^3)(\text{phen})]^+$ cation of **3** optimized at the B3LYP/LACVP+** level of theory. H-atoms were omitted for clarity.

3.4. *In vitro* cytotoxicity

In our previous works dealing with mixed-ligand Cu^{II} complexes²⁰⁻²² involving the CuN_2O_2 donor set, it was demonstrated that the 2-phenyl-3-hydroxy-4(1H)-quinolinone skeleton (Hqui) represents a promising *O,O*-donor ligand for Casiopeínas[®]-like anticancer complexes, which represented the motivation for the herein presented study of **1–5**.

The complexes **1–5**, and *cisplatin* used as a standard, were screened for *in vitro* cytotoxicity against osteosarcoma (HOS), breast adenocarcinoma (MCF7), cervix epitheloid carcinoma (HeLa), malignant melanoma (G361), ovarian carcinoma (A2780), *cisplatin*-resistant ovarian carcinoma (A2780R) as well as non-malignant human fibroblasts (MRC5). In the case of **4**, the testing was limited by low solubility of the complex in the medium used, in this case the IC_{50} was expressed as $>5.0 \mu\text{M}$. Otherwise, all the tested complexes exhibited dose-dependent cytotoxicity against all the cancer cell lines reaching

low-micromolar or sub-micromolar IC_{50} values. Complexes **1–3** and **5** were significantly more cytotoxic (ANOVA, $p < 0.05$) against HOS than *cisplatin* ($IC_{50} = 18.9 \pm 1.7 \mu M$). Against MCF7, only **1** and **2** showed IC_{50} values significantly lower than *cisplatin* ($IC_{50} = 17.9 \pm 3.5 \mu M$). These values are comparable with those obtained for the structurally related complex $[Cu(qui)(phen)]NO_3 \cdot H_2O$ (CuQ), involving non-substituted *qui*, with $IC_{50} = 4.3 \pm 0.1 \mu M$ (HOS) and $7.3 \pm 2.3 \mu M$ (MCF7).²⁰ The viability of HeLa cells, which were not sensitive to *cisplatin* up to the highest tested concentration ($IC_{50} > 50 \mu M$), was reduced comparably by all the complexes, including CuQ ($IC_{50} = 2.9 \pm 0.3 \mu M$). In the case of G361, the IC_{50} values were practically identical for all the tested compounds, including *cisplatin* ($5.8 \pm 2.4 \mu M$). On the other hand, the previously reported CuQ was significantly more active on this cell line with $IC_{50} = 0.8 \pm 0.2 \mu M$. Further, all the tested complexes were found to possess mutually comparable and significantly higher cytotoxicity (ANOVA, $p < 0.05$) than *cisplatin* against A2780. The results showed that the complexes were up to ca. 35-times more effective than *cisplatin* with the best IC_{50} value determined for **5**, i.e. $0.6 \pm 0.1 \mu M$ (*cisplatin*; $21.8 \pm 3.9 \mu M$). Cytotoxicity against A2780R was tested with the aim to uncover the possible ability of the complexes to avoid the resistance of these cells towards *cisplatin* ($IC_{50} > 50 \mu M$). The complexes showed activity in low micromolar IC_{50} ($\approx 3 \mu M$) on this cell line. The difference between IC_{50} determined on A2780 and A2780R was non-significant (ANOVA, $p < 0.05$) for **1** and **3**, which means that the cytotoxic effect was practically of the same extent against both cell lines (Table 1).

To be considered as an anticancer therapeutic candidate, a compound has to be selective for transformed cells over healthy non-transformed cells. In order to assess the cytotoxicity profile of the presented complexes, their toxicity towards non-malignant MRC-5 cells was evaluated. It was found out that the MRC-5 cells showed rather different sensitivity towards the complexes. Complex **1** was comparably cytotoxic against both the transformed and healthy cells, with $IC_{50} = 4.9 \pm 2.7 \mu M$ on MRC-5. Complex **2** showed ca. 3× lower toxicity on MRC-5 than **1** ($IC_{50} = 15.9 \pm 1.2 \mu M$). IC_{50} for complex **3** could not be determined due to its limited solubility in the medium used, therefore its toxicity can be expressed as $IC_{50} > 25 \mu M$. Nevertheless, the result for **3** suggests that there is ca. an order of

magnitude higher cytotoxicity against cancer cells than to healthy cells. The best cytotoxicity profile was found for **5**, which was non-toxic to MRC-5 up to the highest tested concentration ($IC_{50} > 50 \mu M$). The selectivity index (SI) for **5**, calculated as the ratio of $IC_{50}(\text{non-malignant cells})/IC_{50}(\text{A2780})$, is therefore higher than ca. 80, as compared to ca. 2 for *cisplatin* and $SI \approx 40$ for $[Cu(qui)(phen)]BF_4$ (with $IC_{50} = 20.4 \pm 1.2 \mu M$ against primary human hepatocytes).²² Based on the presented results, it can be suggested that the 2-(3,5-dichloro-4-amino)phenyl- and 7-alkylcarboxamido-substitution introduced on the *qui* skeleton resulted in a beneficial cytotoxic profile in the cases of compounds **3** and **5**, but not in the cases of **1** and **2**, therefore highlighting the importance of suitable structural modifications of the *O,O*-ligand in this type of copper(II) complexes. The results of this study clearly showed that optimization of the composition of Cu-quinolinonato complexes can lead to compounds with an increased anticancer effect and simultaneously increased selectivity, which is connected with the suppressed negative side-effects.

Table 1 The results of the *in vitro* cytotoxicity testing of **1–5** and *cisplatin* against the human cell lines. Cells were treated with the tested complexes for 24 h; the measurements were performed in triplicate, and cytotoxicity experiments were repeated in three different cell passages; data are expressed as $IC_{50} \pm SD$ (μM).

Compound	HOS	MCF7	HeLa	G361	A2780	A2780R	MRC-5
1	3.3±1.3	5.5±2.5	3.2±0.3	3.5±0.1	1.0±0.6	2.9±1.2	4.9±2.7
2	4.6±0.2	7.1±2.6	3.0±1.1	3.7±0.5	1.3±0.4	4.4±0.6	15.9±1.2
3	7.1±1.6	>10	4.1±0.8	3.1±0.4	1.9±0.2	2.5±0.7	>25
4	>5	>5	n.t.	n.t.	n.t.	n.t.	n.t.
5	6.7±2.5	31.9±6.4	2.7±0.5	3.2±0.6	0.6±0.1	3.4±0.2	>50
<i>cisplatin</i>	18.9±1.7	17.9±3.5	>50	5.8±2.4	21.8±3.9	>50	>50

n.t. = not tested (due to inactivity in the primary cytotoxicity testing against HOS and MCF7 up to the concentration limited by solubility in the used medium)

Table 2 The results of the EB–DNA fluorescence quenching experiments, including the values of Stern-Volmer quenching constant (K_{SV}) and apparent binding constant (K_{app}) [M^{-1}].

Compound	K_{SV}	K_{app}^*
1	$5.3 \cdot 10^5$	$2.7 \cdot 10^7$
2	$8.5 \cdot 10^4$	$4.2 \cdot 10^6$
3	$8.5 \cdot 10^4$	$4.3 \cdot 10^6$
4	$6.6 \cdot 10^4$	$3.3 \cdot 10^6$
5	$3.2 \cdot 10^4$	$1.6 \cdot 10^6$

* the concentration of EB was 5 μM

3.6. pUC-19 plasmid DNA cleavage

In order to get deeper insight into the mechanisms responsible for the cytotoxicity of the tested copper(II) complexes, the representative complex **5** was tested for the ability to behave as a chemical nuclease in the conditions of oxidative stress, in this case represented by the mixture of hydrogen peroxide and reducing agent (L-ascorbic acid). This model was selected, based on the well-known fact that the overdriven metabolism in tumour cells generates considerable amounts of reactive oxygen and nitrogen species,³⁸ such as superoxide anionic radicals or hydrogen peroxide, which can involve into the generation of highly-toxic hydroxyl species and/or other highly reactive metal-containing species by Fenton reaction.³⁹ The highly-reactive species, like hydroxyl, are able to cause the irreversible damage towards the structure of double-stranded DNA (dsDNA), for example, it can induce the decoupling of nitrogen bases, nick one polynucleotide chain or cleave both strands of DNA.⁴⁰ As a model object, a relatively small circular dsDNA from pUC19 plasmid was used and the ability of the selected representative complex **5** to oxidatively cleave the polynucleotide chains, in the presence of a high excess of hydrogen peroxide, was monitored by gel electrophoresis, which allowed qualitative and quantitative evaluation of different forms of the modified DNA (see Fig. 4).

The quantitative parameter of total DNA cleavage was calculated as a percentage of the integrated densities of cleaved forms (OC-form + 2 x L-form) from the sum of integrated densities of all the identified forms of DNA (CCC-form + OC-form+ 2 x L-form). The results of the quantification are presented in Table 3.

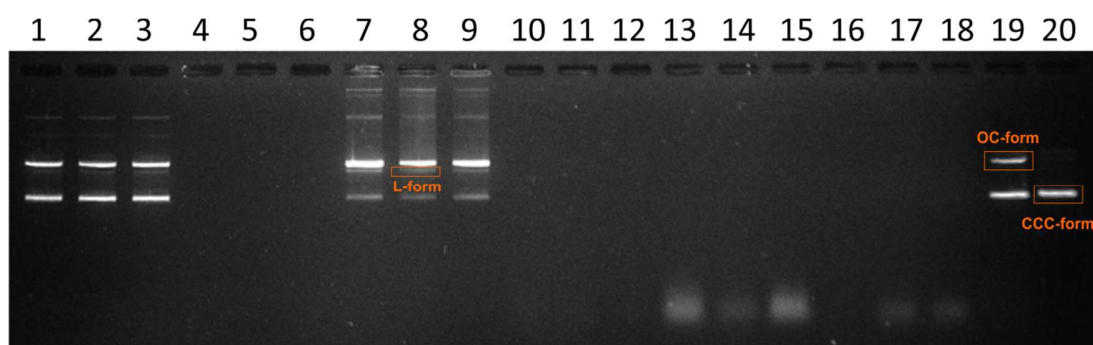


Fig. 4 The electrophoreogram depicting the cleavage of pUC19 plasmid DNA by complex **5** in the presence of hydrogen peroxide. The three basic forms of plasmid DNA are identified as supercoiled DNA (CCC-form), open circular form (OC-form), and linear form (L-form). Lanes 1–3, 7–9 and 13–15 represent the products of the cleavage of pUC19 plasmid induced by the complex **5** applied at the concentrations of 20 μ M, 100 μ M, and 200 μ M, respectively, without addition of ascorbic acid as a reducing agent. Lanes 4–6, 10–12 and 16–18 represent the products of the cleavage of pUC19 plasmid induced by the complex **5** applied at the concentrations of 20 μ M, 100 μ M, and 200 μ M, respectively, with addition of ascorbic acid as a reducing agent (complete cleavage in all cases). Lane 19 represents a blank sample (the mixture of pUC19 plasmid and hydrogen peroxide) and lane 20 represents the native pUC19 plasmid.

Table 3 The results of the DNA-cleavage experiments.

Lane	Concentration of 5	Conditions	CCC [%]	L [%]	OC [%]	Average DNA cleavage [%]
1	20 μ M	w/o L-ascorbic acid	57.1 %	6.9 %	36.0 %	46.3
2			58.1 %	5.7 %	36.2 %	
3			56.8 %	7.7 %	35.5 %	
4	20 μ M	with L-ascorbic acid	0 %	0 %	0 %	100
5			0 %	0 %	0 %	
6			0 %	0 %	0 %	
7	100 μ M	w/o L-ascorbic acid	28.7 %	13.8 %	57.5 %	75.6
8			24.7 %	18.0 %	57.3 %	
9			29.7 %	10.3 %	60.0 %	
10	100 μ M	with L-ascorbic acid	0 %	0 %	0 %	100
11			0 %	0 %	0 %	
12			0 %	0 %	0 %	
13	200 μ M	w/o L-ascorbic acid	0 %	0 %	0 %	100
14			0 %	0 %	0 %	
15			0 %	0 %	0 %	
16	200 μ M	with L-ascorbic acid	0 %	0 %	0 %	100
17			0 %	0 %	0 %	
18			0 %	0 %	0 %	
19	Blank		68.1 %	0 %	31.9 %	31.9
20	Native plasmid		94.7 %	1.2 %	4.1 %	6.4

The results of cleavage experiments showed remarkable ability of complex **5** to cleave the DNA by oxidative mechanism in the presence of the reducing agent (L-ascorbic acid) and even at the smallest concentration used (20 μ M), the complete cleavage of DNA molecules to small fragments occurred, leaving no trace of them in the electrophoregrams (see lanes 4–6, and 10–12 in Fig. 4). At higher concentrations of the complex, the DNA fragments were cross-linked into the structures of higher order (and lower electrophoretic mobility) and therefore, the smear has been detected in the electrophoreogram (see lanes 13–18 in Fig. 4). Complex **5** showed, however, the ability to cleave the polynucleotide chains of dsDNA also without the addition of the reducing agent, reaching the DNA cleavage up to ca. 80% at 100 μ M concentration. At the concentration of 200 μ M, even without the presence of the reducing agent, the complete cleavage of DNA occurred (see lanes 16–18 in Fig. 4).

In conjunction with the above presented results of EB-displacement method, in which complex **5** showed the ability to effectively substitute ethidium bromide at the intercalating site in the minor groove of the DNA double-helix, it can be speculated that the mechanism of DNA-cleavage mediated by this complex is based on the sequence non-specific interaction of the cations $[\text{Cu}(\text{qui})(\text{phen})]^+$, or the similar cationic species containing the $\{\text{Cu}(\text{phen})\}$ residue (see *Section 3.7., Interactions with Sulphur-Containing Biomolecules Assessed by ESI-MS*), with the phosphate moieties, and partly on the intercalation to the minor groove of the double helical DNA,^{41,42} reduction of Cu(II) to Cu(I), and Fenton reaction mediated production of reactive oxygen species that are able to cleave the polynucleotide chains, probably at the C1' or C4' sites of the adjacent deoxyribose moiety.⁴⁰

3.7. Interactions with sulphur-containing biomolecules assessed by ESI-MS

With the aim to describe the interactions of the complexes (on an example of the representative complex **5**) in the solutions at the conditions closer to real physiological environment, we performed the mass spectrometric evaluation of the interacting systems, containing 10 μM of complex **5** and the mixture of L-cysteine and L-glutathione (at 290 μM and 6 μM concentration, respectively) at physiological concentrations.³⁰ The mass spectra of this system were measured immediately after mixing of the components (0h) and then after 1, 12, and 24 h. The most pronounced changes were found after 24 h of interactions (see Fig. 5). The mass spectrum of the interacting system was compared to that of complex **5**, dissolved in methanol:water (1:1, v/v) (see Fig. 5B), which contained a rich variety of peaks, corresponding to the ionic species derived from the *phen* ligand (at 181.17 m/z) and solvated $\{\text{Cu}(\text{phen})\}$ residues, such as $[\text{Cu}(\text{phen})_2+\text{H}]^{2+}$ at 211.67 m/z , $[\text{Cu}(\text{phen})]^+$ at 243.08 m/z , $[\text{Cu}(\text{phen})+\text{H}_2\text{O}+\text{OH}]^+$ at 278.08 m/z , $[\text{Cu}(\text{phen})+\text{H}_2\text{O}+\text{NO}_3+\text{CH}_3\text{OH}+\text{H}]^+$ at 356.00 m/z , $[\text{Cu}(\text{phen})_2+\text{H}]^+$ at 423.17 m/z , $[\text{Cu}(\text{phen})_2+\text{H}_2\text{O}+\text{NO}_3+\text{CH}_3\text{OH}+\text{H}]^+$ at 536.00 m/z , and $[\text{M}-\text{NO}_3]^+$ at 711.08 m/z . In addition to the above mentioned ionic species, the mass spectrum of the interacting system (see Fig. 5C), containing the L-cysteine and L-glutathione, showed one additional set of peaks,

corresponding to the interacting species containing the L-cysteine residue with the composition $[\text{Cu}(\text{qui}^5)+\text{Cys}+\text{H}]^+$ at 667.92 m/z .

The described set of interactions in solutions might contribute significantly to the behaviour of prepared complexes in biological systems leading to their higher affinity in context of DNA binding in the form of the $\{\text{Cu}(\text{phen})\}$ containing species. These findings are in agreement with those reported previously in our works.²⁰⁻²²

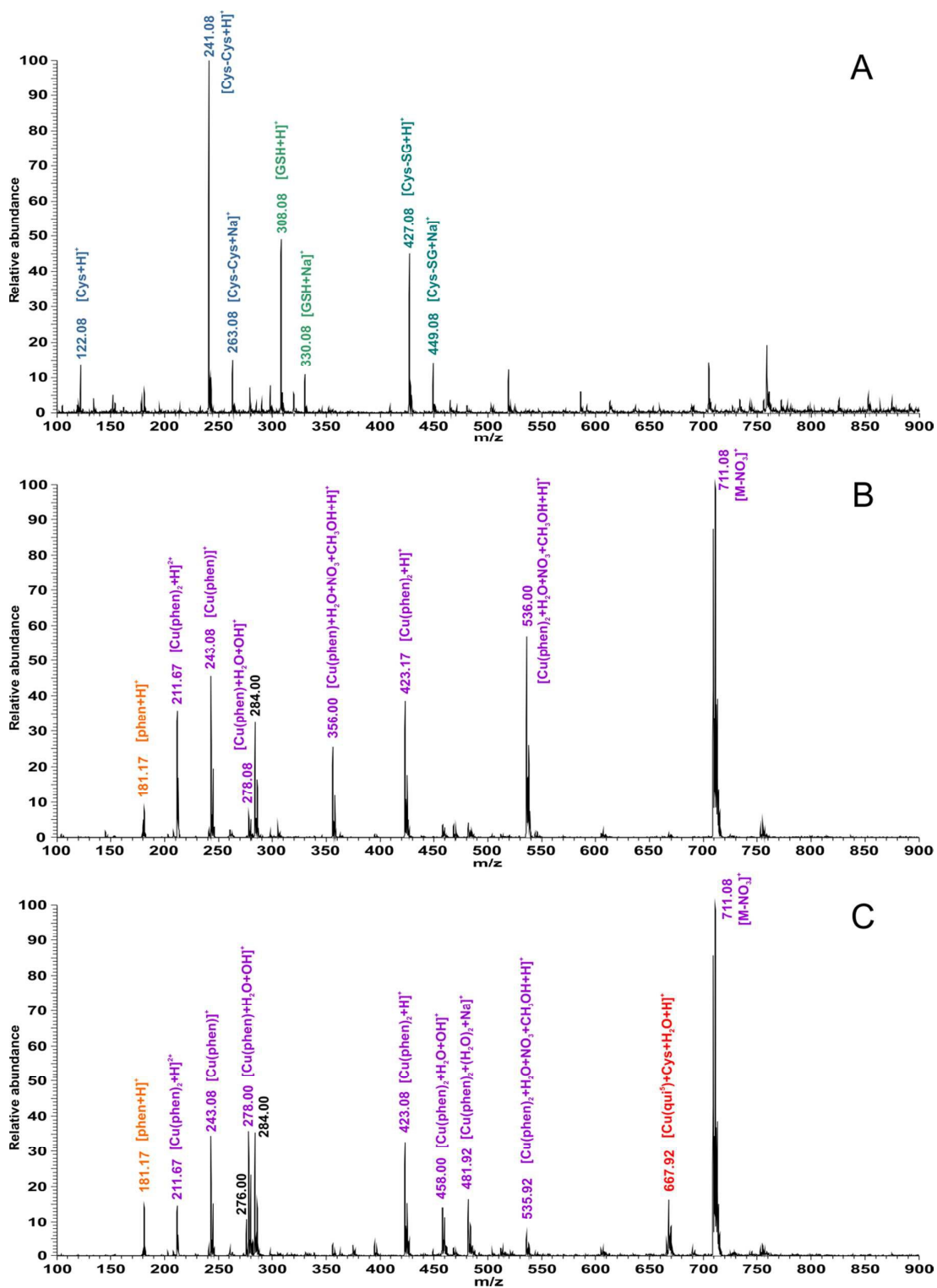


Fig. 5 Results of the ESI-MS study of interactions of complex 5 with the physiological concentrations of L-cysteine and L-glutathione. ESI-MS spectra of the mixture containing the physiological concentrations of L-cysteine and L-glutathione (A), the 10 μM solution of complex 5 in

methanol:water (1:1, v/v), 24 h after preparation (B), and the interacting system containing complex **5** (at the concentration of 10 μM), L-cysteine (at the concentration of 290 μM) and reduced glutathione (at the concentration of 6 μM) (C). The identified ionic species for the selected peaks are indicated.

4. Conclusions

Five copper(II) mixed-ligand complexes with the general composition $[\text{Cu}(\text{qui}^x)(\text{phen})]\text{NO}_3 \cdot y\text{H}_2\text{O}$ (**1–5**), where Hqui^x stands for variously *N*-substituted 2-(4-amino-3,5-dichlorophenyl)-3-hydroxy-4(1*H*)-quinolinone-7-carboxamides; *phen* = 1,10-phenanthroline and *y* = 0–1, were prepared, thoroughly characterized and screened for their *in vitro* cytotoxicity on a panel of human cancer cell lines (HOS, MCF7, HeLa, G361, A2780, A2780R). Additionally, their toxicity to healthy cells was evaluated on a non-malignant lung fibroblast cell line MRC-5. The presented complexes, except for **4**, were found to be potent *in vitro* anticancer agents, with the best IC_{50} value for complex **5**, i.e. 0.6 ± 0.1 μM against A2780. Moreover, complex **5** showed very favourable selectivity index, calculated as the ratio of $\text{IC}_{50}(\text{MRC-5})/\text{IC}_{50}(\text{A2780})$, reaching the value higher than ca. 80. The complexes **1–5** were able to bind to CT-DNA, as evidenced by significant fluorescence quenching of the ethidium bromide-DNA system with the binding constants comparable to ethidium bromide. Furthermore, the pUC19 plasmid DNA cleavage experiments showed the ability of the prepared complexes to act as chemical nucleases in the presence of hydrogen peroxide, and the addition of reducing agent (L-ascorbic acid) increased significantly their pro-oxidative effect. The results of the mass spectrometric evaluation of interactions of the representative complex **5** with the sulphur-containing biomolecules confirmed the ability of the complex to interact with the physiological levels of L-cysteine and simultaneously suggested that the species responsible for the biological activities of the prepared complexes may be associated with the existence of $[\text{Cu}(\text{qui})(\text{phen})]^+$ or similar cationic species containing the $\{\text{Cu}(\text{phen})\}$ moiety.

The reported study unambiguously demonstrated the importance of suitable structural modifications of the *O,O*-ligands in the Casiopeínas[®]-like copper(II) complexes. The results of the most promising complex **5** suggested that the introduced 7-(*p*-xylyl)carboxamido-substitution on the *qui* skeleton resulted in a more beneficial cytotoxic profile with comparable anticancer activity and significantly increased selectivity towards cancer cells over non-malignant cells. In conclusion, it can be pointed out that the presented results represent a next successful step in optimization of composition of Cu-quinolinonato complexes leading to potentiation of their anticancer activity and concurrently suppression of negative side-effects.

Acknowledgements

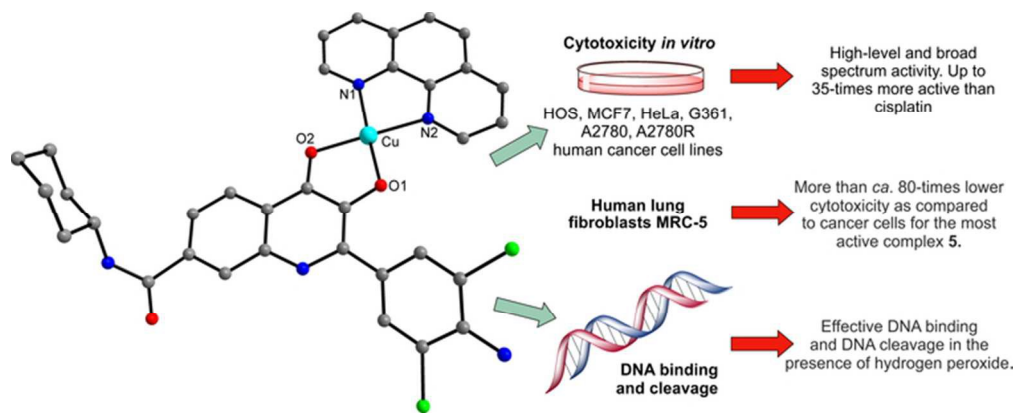
The authors would like to acknowledge the financial support from the National Program of Sustainability I (LO1305) of the Ministry of Education, Youth and Sports of the Czech Republic and Palacký University (PrF_2015_019). We are also grateful to Ms. Kateřina Kubešová for help with cytotoxicity testing, Dr. Bohuslav Drahoš for help with mass spectrometry experiments and Mr. Jakub Hutýra for performing DNA cleavage experiments.

References

- 1 L. R. Kelland and N. P. Farrell, *Platinum Based Drugs in Cancer Therapy*, Humana Press, Totowa, NJ, USA, 2000.
- 2 M. Gielen and E. R. T. Tiekink, *Metallotherapeutic Drugs and Metal-Based Diagnostic Agents*, John Wiley & Sons, Ltd., Chichester, UK, 2005.
- 3 E. Alessio, *Bioinorganic Medicinal Chemistry*, Wiley-VCH Verlag GmbH & Co. KGaA, Weinheim, Germany, 2011.
- 4 P. Heffeter, U. Jungwirth, M. Jakupec, C. Hartinger, M. Galanski, L. Elbling, M. Micksche, B. Keppler and W. Berger, *Drug Resist. Updates*, 2008, **11**, 1.
- 5 X. Y. Wang and Z. J. Guo, *New Trends and Future Developments of Platinum-Based Antitumor Drugs in Bioinorganic Medicinal Chemistry*, ed. E. Alessio, WILEY-VCH Verlag GmbH & Co. KGaA, Weinheim, 2011.
- 6 C. X. Zhang and S. J. Lippard, *Curr. Opin. Chem. Biol.*, 2003, **7**, 481.
- 7 M. C. Linder, *Biochemistry of Copper*, Plenum Press, New York, 1991.
- 8 J. M. C. Gutteridge, *Medical Biology*, 63 (1985) 41–42.
- 9 W. Zhou, X. Wang, M. Hu, C. Zhu and Z. Guo, *Chem. Sci.*, 2014, **5**, 2761.
- 10 S. Tardito, A. Barilli, I. Bassanetti, M. Tegoni, O. Bussolati, R. Franchi-Gazzola, C. Mucchino and L. Marchio, *J. Med. Chem.*, 2012, **55**, 10448.
- 11 D. Palanimuthu, S. V. Shinde, K. Somasundaram and A. G. Samuelson, *J. Med. Chem.*, **5**, 2013, 722.
- 12 C. Marzano, M. Pellei, F. Tisato and C. Santini, *Anti-Cancer Agents Med. Chem.*, 2009, **9**, 185.
- 13 F. P. Dwyer, E. Mayhew, E. M. Roe and A. Shulman, *Br. J. Cancer*, 1965, **19**, 195.
- 14 C. Mejia and L. Ruiz-Azuara, *Pathol. Oncol. Res.*, 2008, **14**, 467.
- 15 M.E. Bravo-Gomez, J. C. Garcia-Ramos, I. Garcia-Mora and L. Ruiz-Azuara, *J. Inorg. Biochem.*, 2009, **103**, 299.

- 16 L. Becco, A. Rodriguez, M. E. Bravo, M. J. Prieto, L. Ruiz-Azuara, B. Garat, V. Moreno and D. Gambino, *J. Inorg. Biochem.*, 2012, **109**, 49.
- 17 A. G. Gutierrez, A. Vazquez-Aguirre, J. C. Garcia-Ramos, M. Flores-Alamo, E. Hernandez-Lemus, L. Ruiz-Azuara and C. Mejia, *J. Inorg. Biochem.*, 2013, **126**, 17.
- 18 G. Vértiz, L.E. García-Ortuno, J.P. Bernal, M.E. Bravo-Gómez, E. Lounejeva, A. Huerta and L. Ruiz-Azuara, *Fund. Clin. Pharmacol.*, 2014, **28**, 78.
- 19 L. Becco, J. C. García-Ramos, L. Ruiz Azuara, D. Gambino and B. Garat, *Biol. Trace Elem. Res.*, 2014, **161**, 210.
- 20 R. Buchtík, Z. Trávníček, J. Vančo, R. Herchel and Z. Dvořák, *Dalton Trans.*, 2011, **40**, 9404.
- 21 R. Buchtík, Z. Trávníček and J. Vančo, *J. Inorg. Biochem.*, 2012, **116**, 163.
- 22 Z. Trávníček, J. Vančo, J. Hošek, R. Buchtík and Z. Dvořák, *Chem. Centr. J.*, 2012, **6**, 160.
- 23 M. Sural, J. Hlaváč, P. Funk, P. Džubák and M. Hajdúch, *ACS Comb. Sci.*, 2011, **13**, 39.
- 24 M. Sural, J. Hlaváč, P. Hradil, I. Fryšová, M. Hajdúch, V. Bertolasi and M. Maloň, *Eur. J. Med. Chem.*, 2006, **41**, 467.
- 25 A.D. Becke, *J. Chem. Phys.*, 1993, **98**, 1372.
- 26 V. Rassolov, J.A. Pople, M. Ratner, P.C. Redfern and L.A. Curtiss, *J. Comput. Chem.*, 2001, **22**, 976.
- 27 V. Shao, L.F. Molnar, Y. Jung, J. Kussmann, C. Ochsenfeld, S.T. Brown, A.T.B. Gilbert, L.V. Slipchenko, S.V. Levchenko, D.P. O'Neill, R.A. DiStasio, Jr., R.C. Lochan, T. Wang, G.J.O. Beran, N.A. Besley, J.M. Herbert, C.Y. Lin, T. Van Voorhis, S.H. Chien, A. Sodt, R.P. Steele, V.A. Rassolov, P.E. Maslen, P.P. Korambath, R.D. Adamson, B. Austin, J. Baker, E.F.C. Byrd, H. Dachsel, R.J. Doerksen, A. Dreuw, B.D. Dunietz, A.D. Dutoi, T.R. Furlani, S.R. Gwaltney, A. Heyden, S. Hirata, C.P. Hsu, G. Kedziora, R.Z. Khalliulin, P. Klunzinger, A.M. Lee, M.S. Lee, W.Z. Liang, I. Lotan, N. Nair, B. Peters, E.I. Proynov, P.A. Pieniazek, Y.M. Rhee, J. Ritchie, E. Rosta, C.D. Sherrill, A.C. Simmonett, J.E. Subotnik, H.L. Woodcock III, W. Zhang, A.T. Bell, A.K. Chakraborty, D.M. Chipman, F.J. Keil, A. Warshel, W.J. Hehre, H.F. Schaefer, J. Kong, A.I. Krylov, P.M.W. Gill and M. Head-Gordon, *Phys. Chem. Chem. Phys.*, 2006, **8**, 3172.

- 28 QC Expert 3.2, Statistical software, TriloByte Ltd., Pardubice, Czech Republic, 2009.
- 29 A. Banerjee, J. Singh and D. Dasgupta, *J. Fluoresc.*, 2013, **23**, 745.
- 30 G. Salemi, M.C. Gueli, M. D'Amelio, V. Saia, P. Mangiapane, P. Aridon, P. Ragonese and I. Lupo, *Neurol. Sci.*, 2009, **30**, 361.
- 31 E.I. Solomon and A.B.P. Lever, *Inorganic Electronic Structure and Spectroscopy, Applications and Case Studies*, vol. 2, Wiley, New York, 1999.
- 32 K. Nakamoto, *Infrared and Raman Spectra of Inorganic and Coordination Compounds, Part B: Applications in Coordination Organometallic and Bioinorganic Chemistry*, fifth ed., Wiley, New York, 1997.
- 33 A. Barve, A. Kumbhar, M. Bhat, B. Joshi, R. Butcher, U. Sonawane and R. Joshi, *Inorg. Chem.*, 2009, **48**, 9120.
- 34 L. Gasque, G. Medina, L. Ruiz-Ramírez and R. Moreno-Esparza, *Inorg. Chim. Acta*, 1999, **288**, 106.
- 35 D. Suh and J. B. Chaires, *Bioorg. Med. Chem.*, 1995, **3**, 723.
- 36 G. Zhao, H. Lin, S. Zhu, H. Sun and Y. Chen, *J. Inorg. Biochem.*, 1998, **70**, 219.
- 37 R.F. Pasternack, M. Caccam, B. Keogh, T.A. Stephenson, A.P. Williams and E.J. Gibbs, *J. Am. Chem. Soc.*, 1991, **113**, 6835.
- 38 J.C. Tung, J.M. Barnes, S.R. Desai, C. Sistrunk, M.W. Conklin, P. Schedin, K.W. Eliceiri, P.J. Keely, V.L. Seewaldt and V.M. Weaver, *Free Radic. Biol. Med.*, 2015, **79**, 269.
- 39 M.L. Kremer, *Phys. Chem. Chem. Phys.*, 1999, **1**, 3595.
- 40 P.C. Dedon, *Chem. Res. Toxicol.*, 2008, **21**, 206.
- 41 A.S. Kumbhar, S.G. Damle, S.T. Dasgupta, S.Y. Rane and A.S. Kumbhar, *J. Chem. Res.-Synop.*, 1999, 98.
- 42 A. Silvestri, G. Barone, G. Ruisi, M. T. Lo Giudice and S. Tumminello, *J. Inorg. Biochem.*, 2004, **98**, 589.



32x12mm (600 x 600 DPI)